materials

MDPI

Article

Ferromagnetic Half-Metal Cyanamides $Cr(NCN)_2$ Predicted from First Principles Investigation

Zhilue Wang [1], Shoujiang Qu [1], Hongping Xiang [1,*], Zhangzhen He [2,*] and Jun Shen [1]

[1] School of Materials Science and Engineering, Tongji University, 4800 Caoan Road, Shanghai 201804, China; wangzl@tongji.edu.cn (Z.W.); qushoujiang@tongji.edu.cn (S.Q.); junshen@tongji.edu.cn (J.S.)

[2] State Key Laboratory of Structural Chemistry, Fujian Institute of Research on the Structure of Matter, Chinese Academy of Sciences, Fuzhou 350002, China

* Correspondence: xianghp@tongji.edu.cn (H.X.); hezz@fjirsm.ac.cn (Z.H.)

Received: 2 March 2020; Accepted: 9 April 2020; Published: 11 April 2020

Abstract: The stability, physical properties, and electronic structures of $Cr(NCN)_2$ were studied using density functional theory with explicit electronic correlation (GGA+*U*). The calculated results indicate that $Cr(NCN)_2$ is a ferromagnetic and half-metal, both thermodynamically and elastically stable. A comparative study on the electronic structures of $Cr(NCN)_2$ and CrO_2 shows that the Cr atoms in both compounds are in one crystallographically equivalent site, with an ideal 4+ valence state. In CrO_2, the Cr atoms at the corner and center sites have different magnetic moments and orbital occupancies, moreover, there is a large difference between the intra- (12.1 meV) and inter-chain (31.2 meV) magnetic couplings, which is significantly weakened by C atoms in $Cr(NCN)_2$.

Keywords: first principles theory; transition metal compounds; magnetism

1. Introduction

Recently, high-valence chromium oxides have attracted much attention because of their unusual physical properties and complicated microscopic mechanism [1–8]. For example, $CaCrO_3$ as a rare metallic antiferromagnet was reported to have a Bose–Einstein condensate at T_N [2,5]. The quasi-one-dimensional Hollandite-type structure $K_2Cr_8O_{16}$ undergoes an unconventional metal–insulator transition while maintaining the ferromagnetic state [3,8]. CrO_2, as a simplest Cr^{4+} compound, is a half-metal ferromagnet (T_C = 390 K) and has been widely used in magnetic recording media. It has been widely studied both in experiment and theory; however, the origin of its half-metal ferromagnetism remains controversial and unclear. Early theoretical studies suggest a self-doping double exchange mechanism for describing the material's intertwined metallicity and ferromagnetism [9,10]. Shim et al. indeed observed two different Cr ions coexistence in CrO_2 using ^{53}Cr nuclear magnetic resonance (NMR), supporting the self-doping and double exchange mechanism [11]. Latterly, Takeda et al. also observed the presence of two Cr sites using the orbital-resolved NMR method, however, they revealed that two Cr ions at the corner and body center sites have the same valence state, but different orbital occupancies [12]. A local orbital order takes place with breaking of the local symmetry. They ascribed it to the negative charge transfer between chromium and oxygen ions. Nevertheless, a realistic low-energy model derived from the first principles calculations presents that the direct exchange interactions and the magnetic polarization of the oxygen 2*p* band play a very important role in the stability of the ferromagnetic ground state of CrO_2 instead of double exchange [13–15]. Thus, a clear and uniform microscopic model is desired to elucidate it.

Here, we predicted a new Cr^{4+}-based compound $Cr(NCN)_2$ by first principles theory. It has a tetragonal structure with a space group of $P4_2/mnm$, similar t-o CrO_2. NCN^{2-} as a pseudochalcogen umligand, has the same oxidation state as O^{2-}, but different structure and electronegative. Experimental

reports indicate that NCN^{2-}-based 3*d* transition-metal compounds display rich physical and chemical properties, showing the similarity and difference to corresponding oxides [16–19]. For instance, Cr_2NCN_3 has the same crystal structure as Cr_2O_3 with the *R*–3*c* space group; however, it is a rare ferromagnetic semiconductor, quite different from antiferromagnetic Cr_2O_3 [17].

As in CrO_2, Cr atoms in $Cr(NCN)_2$ are octahedrally coordinated by nitrogen, forming edge-sharing octahedral ribbons along the *c* axis. However, the octahedra on adjacent ribbons are connected by NCN^{2-}, leading to a larger distance of 5.906 Å, not like those in CrO_2 that share an apex O^{2-} with a shorter distance of 3.450 Å. The large inter-chain distance induces a weak magnetic interaction, and as a result $Cr(NCN)_2$, provides a simpler theoretical model for disclosing the mechanism behind the ferromagnetic and half-metal property for CrO_2, even for other Cr^{4+}-based magnetic compounds. Therefore, in this paper, besides predicting the crystal structure, we also calculated the electronic and magnetic structure through the use of density functional theory with explicit electronic correlation (GGA+*U*). In our study, both GGA and GGA+*U* calculations present a ferromagnetic half-metal for $Cr(NCN)_2$. The electronic structures show the Cr atoms in both $Cr(NCN)_2$ and CrO_2 are in one crystallographically equivalent site, with an ideal 4+ valence state. In CrO_2, the Cr atoms at the corner and center sites have the different magnetic moments and orbital occupancies, moreover, there is a large difference between the intra- (12.1 meV) and inter-chain (31.2 meV) magnetic couplings, which is significantly weakened by C atoms in $Cr(NCN)_2$.

2. Methods

As an AB_2-type compound, two kinds of initial crystal structures were chosen for $Cr(NCN)_2$, that is, tetragonal $P4_2/mnm$ from CrO_2 [20] and orthorhombic Pnnm from the high-pressure CrO_2 and $M(NCNH)_2$ (M = Fe, Co, Ni) [21,22]. This is because, as an analog of O^{2-} ligand, NCN^{2-}-based 3*d* transition metal compounds have been proven to own a similar crystal structure as corresponding oxides [16–19]. The initial structures were optimized by letting all lattice parameters and the positions of Cr, C, and N relax simultaneously until self-consistency was achieved.

The calculations were based on density functional theory [22,23] in which the ground state properties of a many-electron system are determined by an electron density with three spatial coordinates instead of *N* electrons with 3*N* spatial coordinates many-body problem, and performed using the plane–wave pseudopotential Vienna ab initio Simulation Package [24–26], which is a well-tested code and has been successfully used to calculate a great variety of materials [17–19,27–30]. The generalized gradient approximation [31] was used for the exchange-correlation functional, which was formulated by Perdew, Burke, and Ernzerhof (GGA-PBE). The projector-augmented wave (PAW) method was employed with a cutoff energy of 800 eV, which was proposed by Blöchl [32] and implemented by Kresse and Joubert [33]. A uniform mesh grid with an actual spacing of 0.031 $Å^{-1}$ was used to sample the complete Brillouin zone (*k*-point grid of $4 \times 4 \times 10$). Brillouin zone integrations were performed with the Methfessel–Paxton method for structure optimization and the tetrahedron method with Blöchl's correction for electronic structure [34]. The PAW pseudopotentials are $2p^6 3d^5 4s^1$ for Cr, $2s^2 2p^2$ for C, $2s^2 2p^3$ for N, and $2s^2 2p^4$ for O. Electron–electron Coulomb interactions in combination with the self-interaction correction were considered for the Cr atom in the rotationally invariant method (GGA+*U*) with an effective Hubbard parameter $U_{\text{eff}} = U - J$ [35,36], which is set as 3.0 eV, obtained from the previous theoretical studies on the oxides based on Cr^{4+} [6,37].

Density-functional perturbation theory (DFPT) [38] in Vienna ab initio Simulation Package combined with the analysis program PHONOPY [39] was used to calculate the phonon frequencies of $Cr(NCN)_2$. The $2 \times 2 \times 2$ supercell including 112 atoms was used to calculate the force constants. A total of 101 *k*-points was used to sample each segment of band paths in order to obtain phonon dispersion relations.

3. Results and Discussion

The calculated results show that both initial structures ($P4_2/mnm$ and $Pnnm$) are stable in the same ground state, that is, $P4_2/mnm$. Thus, $Cr(NCN)_2$ was predicted to be a tetragonal crystal with the same space group as CrO_2 in ambient condition (Figure 1), and Table S1 in the Supporting Information shows all of the theoretical structure parameters. This is quite similar as the scenario in Cr^{3+} ion-based compound $Cr_2(NCN)_3$, which has the same crystal structure as Cr_2O_3. The calculated lattice parameters are a = 8.04 Å, c = 3.1318 Å, V = 202.445 Å, and Z = 2. The Cr^{4+} ion in the Wyckoff position 2*a* (0 0 0) is coordinated by six nitrogen atoms, leading to a slightly flattened octahedral coordination with four Cr–N bonds at 2.023 Å and two shorter Cr–N bonds at 1.934 Å. The average Cr–N bond length is 1.993 Å, close to the sum of Cr^{4+} and N^{3-} effective ionic radii [40] of 2.01 Å. Edge-sharing CrN_6 octahedra form a single chain along the *z*-axis with a Cr–Cr distance of 3.132 Å (Figure 1). C atoms is in Wyckoff position 4 g (0.2238 0.2238 0) and N atoms occupy in two different positions, that is, N1 4 g (0.1126 0.1126 0) and N2 4 g (0.3299 0.3299 0), forming a strictly linear $[N\text{-}C\text{-}N]^{2-}$ unit (∠N-C-N = 180°). The bond lengths between C and N are 1.264 Å (C-N1) and 1.206 Å (C-N2), indicating the asymmetrical structure of NCN^{2-}. The theoretical predicted $Cr(NCN)_2$ is different from other symmetrical 3*d* transition-metal carbondiimides MNCN (M = Mn, Fe, Co, Ni) and Cr_2NCN_3, in which two C–N bonds are the same, around 1.23 Å. This asymmetric structure results from the coordination of N atoms, N1 is connected by two Cr atoms and one C, but N2 is connected by one Cr and one C. Until now, this asymmetrical structure has only been reported in d^{10} nonmagnetic cyanamides Ag_2NCN [41], HgNCN (II) [42], CdNCN (*R*3*m*) [43], and PbNCN [44]. For example, in Ag_2NCN, there is a single bond C–N 1.270 Å and a triple bond C≡N 1.187 Å. In $Cr(NCN)_2$, the edge-sharing CrN_6 chains are connected by the asymmetrical $[N\text{–}C\equiv N]^{2-}$, as a result of a large distance between CrN_6 chains of about 5.906 Å. Therefore, $Cr(NCN)_2$ would be the first transition-metal cyanamide with partially filled 3*d* orbitals.

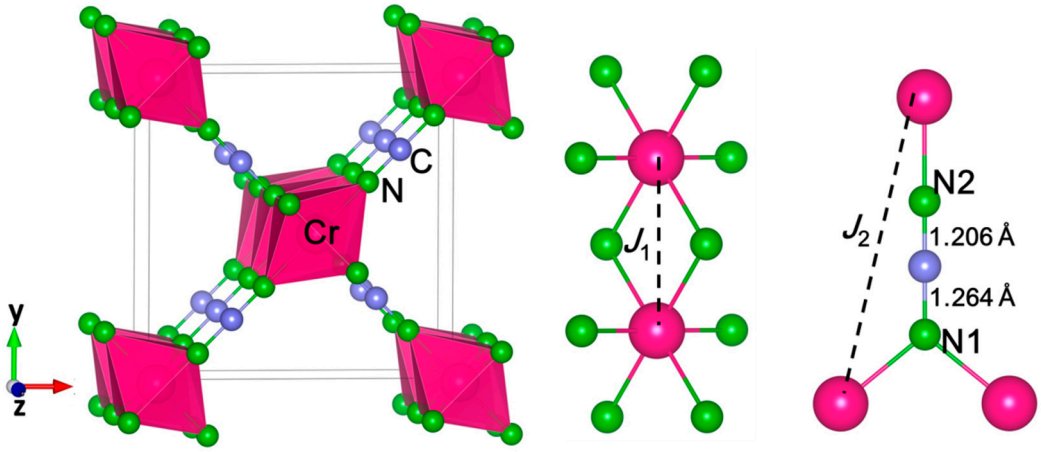

Figure 1. Crystal structures of $Cr(NCN)_2$ (left) and the coordination environments of the Cr^{4+} ion (middle) and the NCN^{2-} ions (right). The Cr, N, and C are in pink, green, and gray, respectively.

The possible reaction routes were summarized in Equations (S1) and (S2) (see Supporting Information), based on successfully synthesized compounds Cr_2NCN_3 and MNCN (M = Mn, Fe, Co, Ni) [16,17]. The calculated reaction energies are −7.46 eV and −4.74 eV, respectively, indicating that the proposed reactions are possible candidates. The formation enthalpy, which is calculated from the direct reaction (Equation (S3)) with elements, is −13.54 eV, suggesting that $Cr(NCN)_2$ is thermodynamically stable relative to the elements. Figure 2 shows the phonon dispersion curves of $Cr(NCN)_2$ in the ferromagnetism, which is the most stable magnetic state and will be discussed below. It has no imaginary modes and hence is dynamically stable.

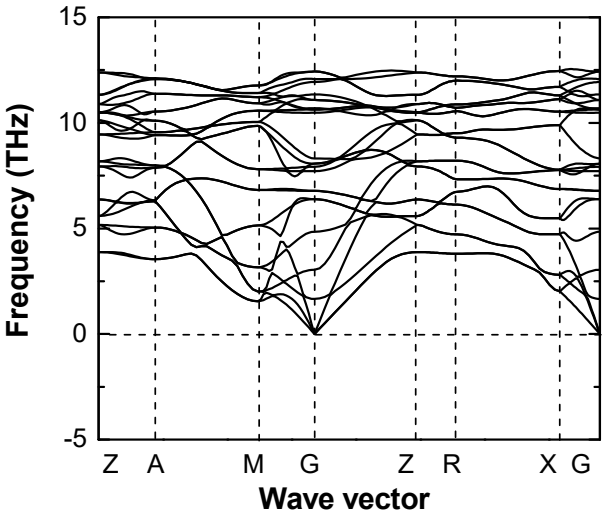

Figure 2. Calculated phonon dispersion relations of $Cr(NCN)_2$ in ferromagnetic state. Imaginary phonon frequencies are shown by negative values.

To achieve quantum-chemical insight into the conductivity and magnetic properties, we performed electronic-structure calculations for $Cr(NCN)_2$ and CrO_2 in $P4_2/mnm$ structure. Considering the structure as shown in Figure 1, two effective magnetic interactions were expected for $Cr(NCN)_2$, the intra-chain J_1 (two neighbors) and inter-chain J_2 (eight neighbors) between the "nearest-neighbor" Cr ions as corresponding to the Cr–N–Cr along CrN_6 octahedral chain and Cr–N–C≡N–Cr superexchange path between chains, respectively (see Figure 1). Thus, we considered a ferromagnetic (FM) and two anti-ferromagnetic structures (AFM1 and AFM2), shown in Figure S1 in the Supporting Information, needed to identify the most probable ground state magnetic structure and estimate the magnitudes of J_1 and J_2. As described in CuNCN [18,19], based on the Heisenberg spin Hamiltonian,

$$\hat{H} = -\sum_{i<j} J_{ij}\hat{S}_i \cdot \hat{S}_j \quad (1)$$

the total energies per unit cell (two formula units) of FM, AFM1, and AFM2 can be written as

$$E_{FM} = (-2J_1 - 8J_2)\left(N^2/4\right) \quad (2)$$

$$E_{AFM1} = (-2J_1 + 8J_2)\left(N^2/4\right) \quad (3)$$

$$E_{AFM2} = 2J_1\left(N^2/4\right) \quad (4)$$

where N is the number of unpaired electrons, $N = 2$ for Cr^{4+} ion. Thus, we can extract J_1 and J_2 from

$$J_2 = (E_{AFM1} - E_{FM})/\left(4N^2\right) \quad (5)$$

$$J_1 = (E_{AFM2} - E_{FM})/\left(N^2\right) - 2J_2 \quad (6)$$

The total energies (Table 1) as calculated from GGA and GGA+U evidence that a ferromagnetic structure is most stable for both $Cr(NCN)_2$ and CrO_2, with the result of CrO_2 consistent with previous experimental and theoretical reports [12,13]. The effective exchange parameters of J_1 and J_2 listed in Table 1 were estimated from the total energies. In the GGA context, the calculated total saturation magnetic moment M_{tot} is 2.01 μ_B f. u. and the spin saturation moment for Cr^{4+} ion M_{Cr} is 2.18 μ_B in $Cr(NCN)_2$, larger than the $S = 1$ scenario. A small negative spin moment about −0.06 μ_B was found for N^{3-}. When including the Coulomb interaction (GGA+U), the M_{tot} increases to 2.26 μ_B f. u., and there present two Cr spin moments of 2.63 μ_B and 2.62 μ_B at the corner Cr1 (0 0 0) and body-center Cr2 (0.5

0.5 0.5) sites, respectively, with a small difference about 0.01 μ_B. Accordingly, the spin moments of N^{3-} diverge to four different values, with an average of −0.11 μ_B. The similar values of J_1 and J_2 calculated from the GGA+U calculation suggest that the couplings of the intra- and inter-chain are comparative.

For CrO_2, GGA and GGA+U both present different spin saturation moments for Cr1 and Cr2, that is, 2.11 μ_B and 2.05 μ_B (GGA), and 2.38 and 2.31 (GGA+U), respectively, with the difference of 0.06 and 0.07 μ_B, respectively. The apex and basal plane oxygens of the CrO_6 octahedron also have different spin moments of −0.05 μ_B and −0.06 μ_B for GGA, and −0.13 μ_B and −0.12 μ_B for GGA+U, respectively. The total saturation magnetic moment increases to 2.09 μ_B in GGA+U from 1.97 in GGA. Obviously, Cr1 and Cr2 in CrO_2 are nonequivalent in magnetism in spite of one crystallographic Cr site, nevertheless, this nonequivalence is not obvious in iso-structure $Cr(NCN)_2$. The values of J_1 and J_2 calculated from the GGA+U calculation are 12.1 and 31.2 meV, respectively. This indicates that the coupling of the inter-chain is stronger than that of the intra-chain.

Table 1. Total energies (E_{total}) (meV) of the ferromagnetic (FM), anti-ferromagnetic (AFM)1, and AFM2 states per formula unit relative to that of the FM state for $Cr(NCN)_2$ and CrO_2; the effective exchange coupling constants (C) (meV); the calculated saturated magnetic moment (M) of Cr, N, and O ions; and the total magnetic moment per formula unit (μ_B), as coming from the GGA and density functional theory with explicit electronic correlation (GGA+U) (U = 3 eV) calculations.

		$Cr(NCN)_2$		CrO_2	
		GGA	**GGA+U**	**GGA**	**GGA+U**
E_{total} **(meV)**	**FM**	0	0	0	0
	AFM1	109.1	172.3	159.6	249.5
	AFM2	57.9	127.2	115.1	148.9
C **(meV)**	J_1	1.7	20.5	17.7	12.1
	J_2	13.7	21.5	19.9	31.2
M (μ_B)	M_{Cr}	2.18	2.63	2.11	2.38
		2.18	2.62	2.05	2.31
	$M_{N/O}$	−0.06	−0.11	−0.05	−0.13
		−0.06	−0.10	−0.06	−0.12
		−0.06	−0.12		
		−0.06	−0.11		
	M_{total}	2.01	2.26	1.97	2.09

The scenario of two Cr sites (corner and center sites) with different spontaneous moments has been reported for CrO_2 in experiments [9–11]. However, two different microscopic mechanisms are proposed: (1) a mixed valence state of $Cr^{+4\pm\delta}$ resulting from a self-doping effect activates the double exchange mechanism, and thus induces the metallic ferromagnetism [9–11]; (2) the two Cr sites do not have different valence states, but have 3d orbital occupation numbers different from each other owing to the negative charge transfer between chromium and oxygen ions; as a result, a local orbital order takes place with breaking of the local symmetry, leading to the difference between the body-center and corner Cr sites [12]. In our calculation, Cr1 and Cr2 in both CrO_2 and $Cr(NCN)_2$ are in one crystallographically equivalent site, with ideal 4+ valence states. Clearly, the nonequivalent magnetic sites do not result from the mixed valence states. In order to disclose the physical mechanism, we perform electronic-structure calculations in the following.

The local density-of-states (DOS) within the FM states of $Cr(NCN)_2$ and CrO_2, as derived from GGA and GGA+U theory, are shown in Figure 3, with the band structure shown in Figure S2 in the Supporting Information. In the GGA description for $Cr(NCN)_2$, there is a finite DOS on the Fermi level in majority spin with a strong Cr–N orbital mixing, while for minority spin, there is an energy gap of 0.62 eV between the highest occupied valence bands with N 2p character and the lowest-lying conduction bands of Cr 3d character, a p–d charge transfer insulating property. These suggest that

$Cr(NCN)_2$ is a half-metal compound, with 100% spin polarized thermally induced current at the Fermi level. Upon including an on-site Coulomb interaction (GGA+U), $Cr(NCN)_2$ keeps the half-metallic character, with the p–d charge transfer energy gap increasing to 1.348 eV for the minority spin.

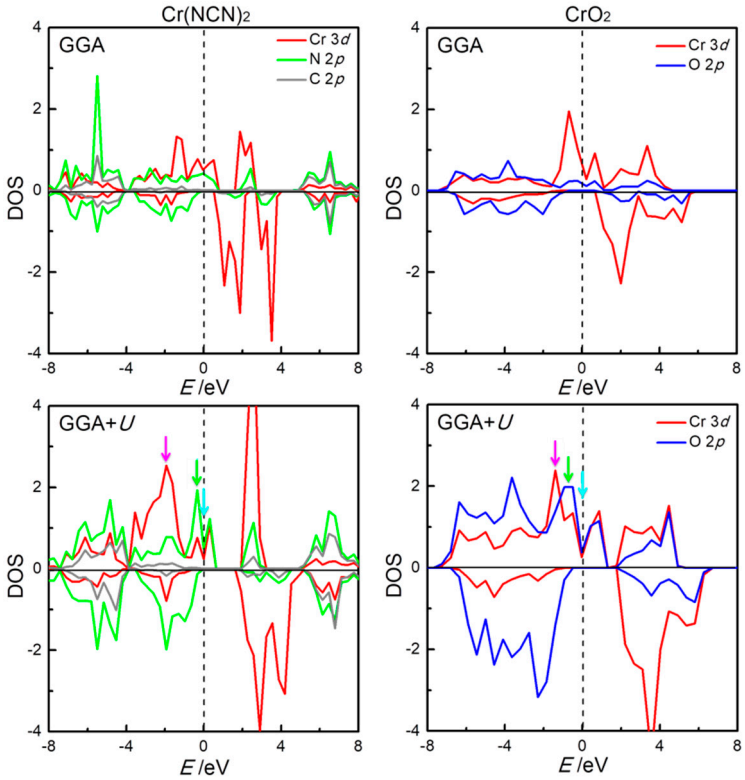

Figure 3. The density-of-states (DOS) of $Cr(NCN)_2$ (left) and CrO_2 (right) projected to Cr 3d (red), N 2p (green), C 2p (grey), and O 2p (blue) orbitals on the basis of GGA (upper row) and density functional theory with explicit electronic correlation (GGA+U) (lower row) calculations. The energy zero indicates the Fermi energy level.

For CrO_2, a half-metallic character is throughout for GGA and GGA+U calculations (Figure 3), in good agreement with experimental reports [12] and previous theoretical study [13]. It is a metallic property for majority spin with a strong Cr–O orbital mixing. For minority spin, the energy gaps of 1.348 and 2.254 eV from GGA and GGA+U theory are found between the highest occupied valence bands with O 2p character and the lowest-lying conduction bands of Cr 3d character, as a p–d charge transfer insulating property. In short, the electronic structures of $Cr(NCN)_2$ from both GGA and GGA+U are similar to those of CrO_2, both of which display the p–d charge transfer half-metal property.

To better understand what is going on with the 3d orbitals of Cr1 (0.5 0.5 0.5) and Cr2 (0 0 0) ions in $Cr(NCN)_2$ and CrO_2, we consider the transformation of the corresponding orbital-projected DOS in more detail. In both compounds, the distortion of CrN_6/CrO_6 results in a symmetry lowering O_h to D_{2h}, that is, a contraction of the octahedron along one of its threefold axes. Therefore, the forms of three t_{2g} orbitals in the global coordinate frame are $|1\rangle = \pm\frac{1}{2}|xy\rangle + \frac{\sqrt{3}}{2}|3z^2 - r^2\rangle$, $|2\rangle = \frac{1}{\sqrt{2}}|yz\rangle \pm \frac{1}{\sqrt{2}}|zx\rangle$, and $|3\rangle = |x^2 - y^2|$ where the "+" and "−" signs stand for Cr1 and Cr2, respectively [13]. Sometimes these orbitals are denoted as $|xy\rangle$, $|yz - zx\rangle$, and $|yz + zx\rangle$ in the local coordinate frame, respectively [45]. The relevant orbital-projected DOS of Cr1 and Cr2 in $Cr(NCN)_2$ and CrO_2 from GGA+U calculations given in Figure 4 are performed on symmetry grounds; we projected densities in majority spin channel of the |1>, |2>, and |3> symmetry with respect to the crystal coordinate frame. We also inserted the numerical orbital populations obtained by integration up to the Fermi energy in Figure 4. In $Cr(NCN)_2$, the projected DOS of |1>, |2>, and |3> of Cr1 and Cr2 are similar, and the orbital populations are quite

close, reflecting almost the same spin moment of Cr1 and Cr2 discussed before. In CrO_2, the projected DOS |1> and |3> of both Cr ions are similar with the close orbital population. However, the projected DOS of |2> of Cr1 and Cr2 are dissimilar, with the difference of 0.226 in the orbital population. Obviously, the different spin moments of Cr1 and Cr2 in CrO_2 mainly result from |2>.

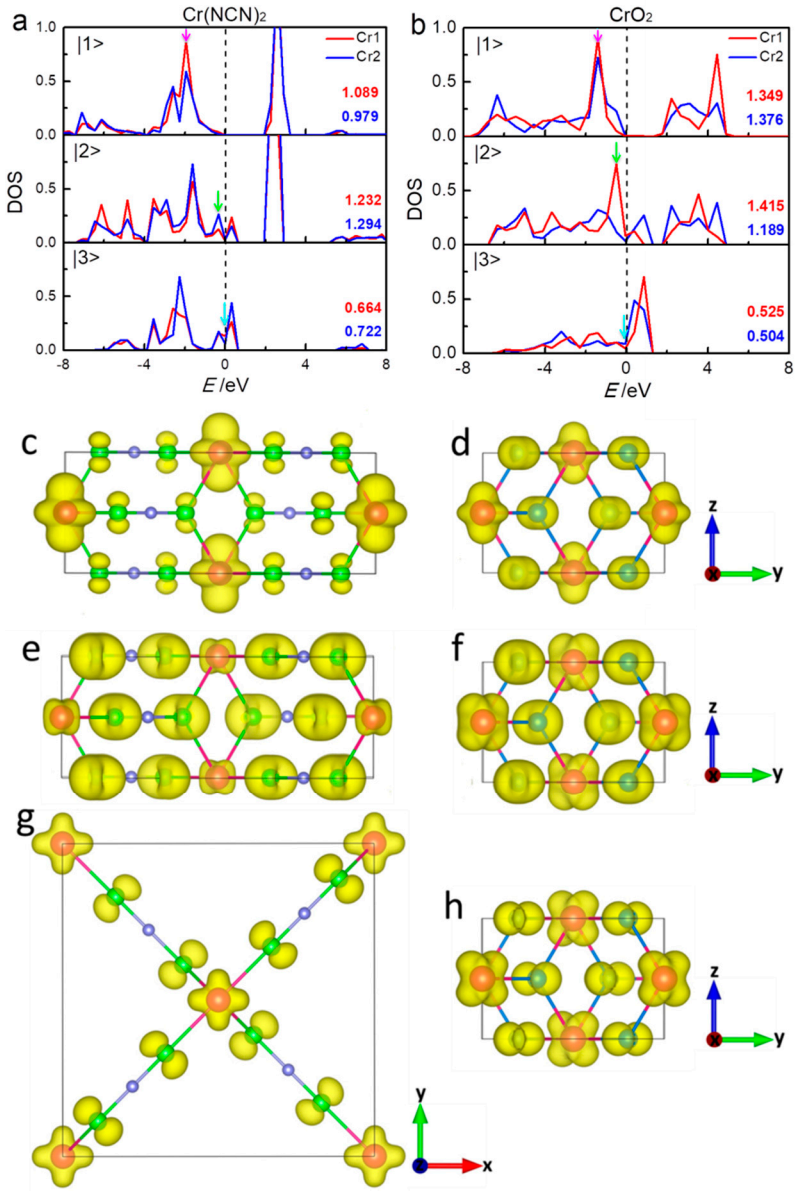

Figure 4. The partial densities-of-states in the spin majority of the Cr 3*d* orbitals on the basis of GGA+*U* calculations for $Cr(NCN)_2$ (**a**) and CrO_2 (**b**). The values inserted are the populations of the five Cr 3*d* orbitals in the majority channels, as calculated by integration (up to Fermi level E_F) of the partial densities-of-states. The energy zero indicates the Fermi energy level. The corresponding three-dimensional electron density contour plots (e/Å^{-3}) in the regions of (–2.20)–(–1.60) eV (**c**), (–0.69)–(–0.40) eV (**e**), and (–0.10)–0.0 eV (**g**) for $Cr(NCN)_2$ and (–1.57)–(–1.35) eV (**d**), (–0.64)–(–0.37) eV (**f**), and (–0.10)–0.0 (**h**) eV for CrO_2 (energy regions shown in blue, green, and purple arrows in Figures 3 and 4a,b).

For both compounds, |1> mainly locates below −1.0 eV and is localized with an energy gap of 1.9 eV for $Cr(NCN)_2$ and 1.3 eV for CrO_2 at the Fermi level. Moreover |1> is less hybridized with O 2*p* orbitals (Figure 3), suggesting a possible direct Cr–Cr interaction. |1> of Cr ions in $Cr(NCN)_2$ have a smaller orbital occupation (1.089 and 0.979) than those in CrO_2 (1.349 and 1.376). In both compounds,

the electrons in |2> and |3> are itinerantly crossing the Fermi level with a strong hybridization with N/O 2*p* orbitals (Figure 3). The Fermi level is mainly occupied by |3> in $Cr(NCN)_2$, while that of CrO_2 is occupied by both |2> and |3>. Besides, |3> in $Cr(NCN)_2$ (0.66 and 0.72) has a bigger orbital population than that in CrO_2 (0.53 and 0.50). The total orbital populations of 3*d* orbitals of Cr1 and Cr2 are 2.985 and 2.995 in $Cr(NCN)_2$, and 3.289 and 3.069 in CrO_2, respectively, larger than 2.0 of ideal Cr^{4+} ion ($3d^2$). That probably implies a large negative charge transfer from N/O 2*p* orbitals to Cr 3*d* orbitals. In short, the different spin moments of Cr1 and Cr2 in CrO_2 mainly result from |2>. The conductivity of $Cr(NCN)_2$ mainly results from |3>, however, that of CrO_2 is attributed from both |2> and |3>.

In order to gain insight into the magnetic coupling between the Cr1 and Cr2 ions, we analyze the three-dimensional electronic-density contour plots near the Fermi level, according to orbital-projected DOS. Figure 4c,d show the density of electron distribution in the energy regions of (–2.20)–(–1.60) eV for $Cr(NCN)_2$ and (–1.57)–(–1.35) eV for CrO_2 (purple arrows in Figure 3 and in bottom panel of Figure 4b). In this region, for both compounds, the electrons are almost occupied in Cr atoms |1> orbitals, forming *d*–*d* direct superexchange in the edge-shared CrN_6/CrO_6 chain. This superexchange, where an electron is assumed to drift from one cation, exists in the compounds with edge-sharing or face-sharing octahedral chain or dimer. The *d*–*d* hopping is very important for early 3*d* meals such as Ti, V, and Cr [46]. As shown in Figure 4a,b, Cr^{4+} ion in both $Cr(NCN)_2$ and CrO_2 has |1> orbital only partially occupied for the up-spin state, that is, the integrated value in the full energy range is around 2, while the orbital occupation (integration below Fermi level) is only around 1, thus an intra-chain ferromagnetic interaction is expected [46,47]. The calculated effective exchange coupling constants of intra-chain J_1 from GGA+*U* (Table 1) are 20.5 and 12.1 meV for $Cr(NCN)_2$ and CrO_2, respectively, indicating a stronger intra-chain coupling in $Cr(NCN)_2$. Figure 4e,f shows the density of electron distribution in the energy regions of (––0.69)–– (–0.40) eV and (–0.64)–(–0.37) eV for $Cr(NCN)_2$ and CrO_2, respectively (green arrows in Figure 3 and middle panel of Figure 4a,b). In this region, the electrons are mainly occupied by Cr |2> orbitals and O 2*p* orbitals, forming *dpπ*–*dpπ* correlation ferromagnetic superexchange between Cr1 and Cr2 sites. In CrO_2, this interaction is strong, while it is cut off by C atoms in $Cr(NCN)_2$. This is consistent with the results of the inter-chain coupling constants J_2 from GGA+*U* calculations, that is, 21.5 meV for $Cr(NCN)_2$ and 31.2 meV for CrO_2. Figure 4g,f show the density of electron distribution in the energy regions near the Fermi level, that is, from −0.10–0.0 eV for $Cr(NCN)_2$ and −0.10–0.0 eV for CrO_2, respectively (blue arrows in Figure 3 and bottom panel of Figure 4a,b). In this region, the electrons are mainly occupied by Cr |3> orbitals and O 2*p* orbitals, also forming *dpπ*–*dpπ* correlation ferromagnetic superexchange between Cr1 and Cr2 sites. However, the electrons are more localized in $Cr(NCN)_2$ than those in CrO_2 because of the large size ligand of NCN^{2-}. Obviously, there are two magnetic couplings, that is, direct *d*–*d* exchange and indirect *dpπ*–*dpπ* superexchange, dominating the ferromagnetic properties of $Cr(NCN)_2$ and CrO_2. In $Cr(NCN)_2$, the strengths of the intra- and inter-chain couplings are comparative, however, in CrO_2, there is a large difference between them, that is, 12.1 meV for intra-chain and 31.2 meV for inter-chain.

4. Conclusions

In summary, on the basis of the results of density functional theory with explicit electronic correlation, $Cr(NCN)_2$ is a ferromagnetic and half-metal material, and stable both thermodynamically and elastically. It was predicted to be a tetragonal structure in the space group of $P4_2/mnm$ with an asymmetrical $[N–C{\equiv}N]^{2-}$ ligand; as a result, it would be the first transition-metal cyanamide with partially filled 3*d* orbitals. A comparative study on the electronic structures of $Cr(NCN)_2$ and CrO_2 presents that the Cr atoms in both compounds are in one crystallographically equivalent site, however, in CrO_2, the Cr atoms at the corner and center sites have different magnetic moments and orbital occupancies, and there is a large difference between the intra- (Cr atoms at the same site) and inter-chain (Cr atoms at the different sites) magnetic couplings. This difference is significantly weakened by C atoms in $Cr(NCN)_2$. Thus, ferromagnetically half-metallic $Cr(NCN)_2$ might be an interesting spintronic material, and we hope it could be synthesized in the future.

Supplementary Materials: The following are available online at http://www.mdpi.com/1996-1944/13/8/1805/s1. Table S1. The structure parameters of predicted $Cr(NCN)_2$. Thermodynamically stability. Figure S1. Ordered spin arrangements of $Cr(NCN)_2$ and CrO_2 designed as (a) FM, (b) AFM1, and (c) AFM2 employed to extract the spin exchange parameters J_1 and J_2. Figure S2. Band structures near the Fermi energy for (a) $Cr(NCN)_2$ and (b) CrO_2 from GGA+U (U = 3 eV) calculations.

Author Contributions: Z.W. and S.Q. performed the experiments; all authors analyzed the data and discussed the results; J.S. analyzed the result; Z.W., H.X., and Z.H. wrote the paper. All authors have read and agreed to the published version of the manuscript.

Funding: This work was supported by the National Natural Science Foundations of China (51601187 and 51971159), and the Natural Science Foundation of Fujian Province (No. 2016J05059).

Conflicts of Interest: The authors declare no conflict of interest. The funders had no role in the design of the study; in the collection, analyses, or interpretation of data; in the writing of the manuscript; or in the decision to publish the results.

References

1. Sakurai, H.; Kolodiazhnyi, T.; Michiue, Y.; Takayama-Muromachi, E.; Tanabe, Y.; Kikuchi, H. Unconventional colossal magnetoresistance in sodium chromium oxide with a mixed-valence state. *Angew. Chem. Int. Ed.* **2012**, *124*, 6757–6760. [CrossRef]
2. Komarek, A.C.; Streltsov, S.V.; Isobe, M.; Möller, T.; Braden, M. CaCrO3: An anomalous antiferromagnetic metallic oxide. *Phys. Rev. Lett.* **2008**, *101*, 167204. [CrossRef] [PubMed]
3. Toriyama, T.; Nakao, A.; Yamaki, Y.; Nakao, H.; Otha, Y. Peierls Mechanism of the metal-insulator transition in ferromagnetic hollandite $K_2Cr_8O_{16}$. *Phys. Rev. Lett.* **2011**, *107*, 266402. [CrossRef] [PubMed]
4. Jin, H.S.; Ahn, K.H.; Jung, M.C.; Lee, K.W. Strain and spin-orbit coupling induced orbital-ordering in mott insulator $BaCrO_3$. *Phys. Rev. B* **2014**, *9*, 205124. [CrossRef]
5. Komarek, A.C.; Möller, T.; Isobe, M.; Drees, Y.; Braden, M. Magnetic order, transport and infrared optical properties in the $ACrO_3$ system (A = Ca, Sr, and Pb). *Phys. Rev. B* **2011**, *84*, 125114. [CrossRef]
6. Cheng, J.G.; Kweon, K.E.; Larregola, S.A.; Ding, Y.; Shirako, Y.; Marshall, L.G.; Li, Z.-Y.; Li, X.; António, M.; Suchomel, M.R.; et al. Charge disproportionation and the pressure-induced insulator-metal transition in cubic perovskite $PbCrO_3$. *Proc. Natl. Acad. Sci. USA* **2015**, *112*, 1670–1674. [CrossRef]
7. Xiao, W.; Tan, D.; Xiong, X.; Liu, J.; Xu, J. Large volume collapse observed in the phase transition in cubic $PbCrO_3$ perovskite. *Proc. Natl. Acad. Sci. USA* **2010**, *107*, 14026–14029. [CrossRef]
8. Hasegawa, K.; Isobe, M.; Yamauchi, T.; Ueda, H.; Ueda, Y. Discovery of ferromagnetic-half-metal-to-insulator transition in $K_2Cr_8O_{16}$. *Phys. Rev. Lett.* **2009**, *103*, 146403. [CrossRef]
9. Korotin, M.A.; Anisimov, V.I.; Khomskii, D.I.; Sawatzky, G.A. CrO_2: A self-doped double exchange ferromagnet. *Phys. Rev. Lett.* **1998**, *80*, 4305–4308. [CrossRef]
10. Schlottmann, P. Double-exchange mechanism for CrO_2. *Phys. Rev. B* **2003**, *67*, 386–393. [CrossRef]
11. Shim, J.H.; Lee, S.; Dho, J.; Kim, D.H. Coexistence of two different Cr Ions by self-doping in half-metallic CrO_2 nanorods. *Phys. Rev. Lett.* **2007**, *99*, 057209. [CrossRef] [PubMed]
12. Takeda, H.; Shimizu, Y.; Kobayashi, Y.; Itoh, M.; Jinno, T.; Isobe, M. Local electronic state in the half-metallic ferromagnet CrO_2 investigated by site-selective ^{53}Cr NMR measurements. *Phys. Rev. B* **2016**, *93*, 235129. [CrossRef]
13. Solovyev, I.V.; Kashin, I.V.; Mazurenko, V.V. Mechanisms and origins of half-metallic ferromagnetism in CrO_2. *Phys. Rev. B* **2015**, *92*, 144407. [CrossRef]
14. Heffernan, K.H.; Yu, S.; Deckoff-Jones, S.; Zhang, X.; Talbayev, D. The role of spin fluctuations in the conductivity of CrO_2. *Phys. Rev. B* **2016**, *93*, 165143. [CrossRef]
15. Toropova, A.; Kotliar, G.; Savrasov, S.Y.; Oudovenko, V.S. Electronic structure and magnetic anisotropy of CrO_2. *Phys. Rev. B* **2005**, *71*, 172403. [CrossRef]
16. Boyko, T.D.; Green, R.J.; Dronskowski, R.; Moewes, A. Electronic band gap reduction in manganese carbodiimide: MnNCN. *J. Phys. Chem. C* **2013**, *117*, 12754–12761. [CrossRef]
17. Tang, X.J.; Xiang, H.P.; Liu, X.H.; Speldrich, M.; Dronskowski, R. A ferromagnetic carbodiimide: $Cr_2(NCN)_3$. *Angew. Chem. Int. Ed.* **2010**, *49*, 4738–4742. [CrossRef]

18. Liu, X.; Dronskowski, R.; Kremer, R.K.; Ahrens, M.; Lee, C.; Whangbo, M. Characterization of the Magnetic and Structural Properties of Copper Carbodiimide, CuNCN, by Neutron Diffraction and First-Principles Evaluations of Its Spin Exchange Interactions. *J. Phys. Chem. C* **2008**, *112*, 11013–11017. [CrossRef]
19. Xiang, H.P.; Liu, X.H.; Dronskowski, R. Theoretical reinvestigation of the electronic structure of CuNCN: The influence of packing on the magnetic properties. *J. Phys. Chem. C* **2009**, *113*, 18891–18896. [CrossRef]
20. Maddox, B.R. High-pressure structure of half-metallic CrO_2. *Phys. Rev. B* **2006**, *73*, 144111. [CrossRef]
21. Tang, X.J.; Houben, A.; Liu, X.H.; Stork, L.; Dronskowski, R. Crystal structure refinement of $M(NCNH)_2$ (M = Fe, Co) based on combined neutron and X-ray diffraction Data. *ZAAC* **2011**, *637*, 1089–1091. [CrossRef]
22. Hohenberg, P.; Kohn, W. Inhomogeneous electron gas. *Phys. Rev. B* **1964**, *136*, 864–871. [CrossRef]
23. Kohn, W.; Sham, L.J. Self-consistent equations including exchange and correlation effects. *Phys. Rev.* **1965**, *140*, A1133. [CrossRef]
24. Kresse, G.; Hafner, J. Ab initio molecular dynamics for open-shell transition metals. *Phys. Rev. B* **1993**, *48*, 13115–13118. [CrossRef] [PubMed]
25. Kresse, G. Efficient iterative schemes for ab initio total-energy calculations using a plane-wave basis set. *Phys. Rev. B* **1996**, *54*, 11169–11186. [CrossRef] [PubMed]
26. Kresse, G.; Furthmüller, J. Efficiency of ab-initio total energy calculations for metals and semiconductors using a plane-wave basis set. *Comput. Mater. Sci.* **1996**, *6*, 15–50. [CrossRef]
27. Altmeyer, M.; Jeschke, H.O.; Hijano-Cubelos, O.; Martins, C.; Lechermann, F.; Koepernik, K.; Santander-Syro, A.F.; Rozenberg, M.; Valenti, R.; Gabay, M. Magnetism, spin texture, and in-gap states: Atomic specialization at the surface of oxygen-deficient $SrTiO_3$. *Phys. Rev. Lett.* **2015**, *116*, 157203. [CrossRef]
28. Beutier, G.; Collins, S.P.; Dimitrova, O.V.; Dmitrienko, V.E. Band Filling Control of the Dzyaloshinskii-Moriya Interaction in Weakly Ferromagnetic Insulators. *Phys. Rev. Lett.* **2017**, *119*, 167201. [CrossRef]
29. Wen, X.D.; Martin, R.L.; Henderson, T.M.; Scuseria, G.E. Density functional theory studies of the electronic structure of solid state actinide oxides. *Chem. Rev.* **2013**, *113*, 1063–1096. [CrossRef]
30. Zheng, S.; Huang, C.; Yu, T.; Xu, M.; Zhang, S.; Xu, H.; Liu, Y.; Kan, E.; Wang, Y.; Yang, G. High-Temperature Ferromagnetism in Fe_3P Monolayer with Large Magnetic Anisotropy. *J. Phys. Chem. Lett.* **2019**, *10*, 2733–2738. [CrossRef]
31. Perdew, J.P.; Burke, K.; Ernzerhof, M. Generalized gradient approximation made simple. *Phys. Rev. Lett.* **1996**, *77*, 3865–3868. [CrossRef] [PubMed]
32. Blochl, P.E. Projector augmented-wave method. *Phys. Rev. B* **1994**, *50*, 17953–17979. [CrossRef] [PubMed]
33. Kresse, G.; Joubert, D. From ultrasoft pseudopotentials to the projector augmented-wave method. *Phys. Rev. B* **1999**, *59*, 1758–1775. [CrossRef]
34. Peter, E.; Jepsen, O.; Andersen, O.K. Improved tetrahedron method for brillouin-zone integrations. *Phys Rev. B* **1994**, *49*, 16223–16233. [CrossRef]
35. Anisimov, V.I.; Poteryaev, A.I.; Korotin, M.A.; Anokhin, A.O.; Kotliar, G. First-principles calculations of the electronic structure and spectra of strongly correlated systems: Dynamical mean-field theory. *J. Phys.-Condens. Matter* **1997**, *9*, 7359–7367. [CrossRef]
36. Dudarev, S.L.; Botton, G.A.; Savrasov, S.Y.; Humphreys, C.J.; Sutton, A.P. Electron-energy-loss spectra and the structural stability of nickel oxide: An LSDA+U study. *Phys. Rev. B* **1998**, *57*, 1505–1509. [CrossRef]
37. Bhobe, P.A.; Chainani, A.; Taguchi, M.; Eguchi, R.; Shin, S. Electronic structure of an antiferromagnetic metal: $CaCrO_3$. *Phys. Rev. B* **2010**, *83*, 165132. [CrossRef]
38. Liu, X.; Müller, P.; Kroll, P.; Dronskowski, R. Synthesis, structure determination, and quantum-chemical characterization of an alternate HgNCN polymorph. *Inorg. Chem.* **2002**, *41*, 4259–4265. [CrossRef]
39. Baroni, S.; Gironcoli, S.; Corso, A.D.; Giannozzi, P. Phonons and related crystal properties from density-functional perturbation theory. *Rev. Mod. Phys.* **2001**, *73*, 515. [CrossRef]
40. Togo, A.; Oba, F.; Tanaka, I. First-principles calculations of the ferroelastic transition between rutile-type and $CaCl_2$-type SiO_2 at high pressures. *Phys. Rev. B* **2008**, *78*, 134106. [CrossRef]
41. Shannon, R.D. Revised effective ionic radii and systematic studies of interatomic distances in halides and chalcogenides. *Acta Crystallogr.* **1976**, *32*, 751–767. [CrossRef]
42. Becker, M.; Nuss, J.; Jansen, M. ChemInform Abstract: Synthesis and characterization of sodium cyanamide. *ChemInform* **2010**, 32. [CrossRef]
43. Baldinozzi, G.; Malinowska, B.; Rakib, M.; Durand, G. Crystal structure and characterisation of cadmium cyanamide. *J. Mater. Chem. A* **2002**, *12*, 268–272. [CrossRef]

44. Cooper, M.J. The structures of some inorganic cyanamides. II. The structure of lead cyanamide. *Acta Crystallogr.* **1964**, *17*, 1452–1456. [CrossRef]
45. Yamasaki, A.; Chioncel, L.; Lichtenstein, A.I.; Andersen, O.K. Model hamiltonian parameters for half-metallic ferromagnets NiMnSb and CrO_2. *Phys. Rev. B* **2006**, *74*, 024419. [CrossRef]
46. Goodenough, J.B. *Magnetism and the Chemical Bond*; Interscience Publishers: New York, NY, USA, 1963; p. 180.
47. Xiang, H.P.; Tang, Y.Y.; Zhang, S.Y.; He, Z. Intra-chain superexchange couplings in quasi-1D 3d transition-metal magnetic compounds. *J. Phys.-Condens. Matter* **2016**, *28*, 276003. [CrossRef]